A High Dynamic Range Ion Detector for the Astral™ Analyzer.

Hamish Stewart[1]*, Johannes Petzoldt[1], Toby Shanley[1], Dmitry Grinfeld[1], Eduard Denisov[1], Bernd Hagedorn[1], Ankit Dwivedi[1], Daniel Mourad[1], Robert Ostermann[1], Maximilian Ochmann[1], Philipp Cochems[1], Alexander Wagner[1], Wilko Balschun[1], Alexander Makarov[1], Semyon Shofman[2], Ben-David Moti[2], Amit Weingarten[2], Sascha Kadyshevitch[2] and Christian Hock[1].

[1]Thermo Fisher Scientific, 11 Hannah-Kunath Str., 28199 Bremen, Germany.

[2]El-Mul Technologies Ltd., Rehovot, Israel

ABSTRACT: Reflectron-based time-of-flight analyzers rely on sub-nanosecond detector time response to achieve acceptable resolving power for low-mid mass, multiple ion peaks. With the adoption of multi-reflection analyzers, order of magnitude longer folded ion paths relax restrictions on detector response time, allowing implementation of new technologies that greatly improve dynamic range, detector lifetime, and ion detection efficiency. A detection system is presented, integrated into the Astral analyzer, that combines 10 keV post-acceleration and focal plane correction with a unique BxE focusing, optically coupled detector, pre-amplification and dual channel digitization. Calibration and peak handling methods are also described. The instrument demonstrated >1x10^4 dynamic range in a single shot, >100k resolving power, and a relative immunity to detector ageing

INTRODUCTION

Mass spectrometers typically detect analyte ions via either inductive detection of trapped ions, or conversion to secondary electrons and multiple subsequent electron multiplication steps to generate measurable current. Ions separated by the mass analyzer are directed with kinetic energy to a conversion surface, and the impact induces emission of secondary electrons, and on some level also secondary ions. The released electrons are then accelerated by an applied electric field to collide with a downstream surface, generating additional electrons, and the process repeated.

Electron multipliers may be formed of either a chain of discrete dynodes or incorporate a continuous dynode such as in channel electron multipliers where a single resistive surface accommodates several electron multiplication steps.

Time-of-Flight (ToF) mass spectrometry is an important technique, widely used in biochemical analysis owing to its high achievable resolving power and speed of measurement. In this form of mass spectrometry, ions are pulse extracted from an injector region, traverse a flight region which commonly includes a reflection stage, and are focused onto the detector's conversion surface[1-3]. The *m/z* resolving power of the analyzer R relates to the total time of flight T and the arrival time spread of the ions ∂T , so that $R = T/2\partial T$. This necessitates a minimization of time-of-flight aberrations for not only ions, but also the secondary and multiplied electrons. For a regular analyzer with 7 keV flight energy and a 2-meter flight path, the time spread for even an *m/z* 1000 ion to achieve 30,000 mass resolution falls well below 1 ns. For lower *m/z* ions having the same flight energy, this pulse-width requirement becomes much more stringent, and the fixed time response of the detector becomes proportionally larger; the primary contributor of resolution loss at low *m/z*. Another matter is that dispersion of the extracted ion packet in flight favors a relatively large conversion surface for acceptable transmission, and that this surface must be well aligned mechanically to the ion packet's focal plane. This requires either ~10 µm level mechanical accuracy over the analyzer[4], mechanical calibration via moving parts[5], or re-alignment of the ion focal plane by electrostatic tilt correction devices[4, 6-7].

Consequently, only detectors with a fast time-response are suitable for conventional time-of-flight analyzers, which also limits the use of peak-broadening pre-amplifiers between detector and analogue-to–digital (ADC) conversion. The multi-channel plate[8] (MCP) is the dominant detector type, owing to its fast response, even down to 0.2 ns, and acceptable lifetime. These are flat plates of resistive material containing an array of millions of µm scale pores that each act as an individual multiplication channel. A stack of two MCPs in series provides sufficient gain, ~10^5 to allow for detection of single ions. The downsides are in handling of the fragile materials, that the typical ~60% proportional coverage of the pores over the total surface area (the open area ratio) impacts detection efficiency, and that high resistance allows for charge depletion and thus restricts dynamic range.

A more recent development has been the introduction of BxE (crossed magnetic and electrostatic field) focusing of secondary electrons, greatly reducing the time aberrations associated with the electron starting position along large dynode surfaces and resulting in large discrete and continuous dynode electron multipliers with a 0.4 ns single ion time response[9].

A weakness of conventional electron multipliers is ageing, whereby the detector's gain falls as the total charge output increases. To a great extent this is compensated by simply increasing the potential across the device, but eventually hits the mechanical limits at which high-voltage breakdowns become inevitable. The ageing is believed to be relate to electron-induced deposition of material, particularly hydrocarbons, from the background vacuum to the multiplier surfaces, increasing the work function as carbon layers are deposited[10]. MCPs may

appear relatively resistant to this effect simply because the work function of the resistive material is much greater than that of coated steel dynodes to begin with.

Photomultiplier tubes (PMTs), themselves electron multipliers nested behind a photocathode, provide for magnitude longer lifetime by sealing the dynode surfaces and protecting them from the background material of the instrument vacuum. Hybrid photodetectors incorporating both ion conversion to electrons, a scintillator and an optically coupled PMT thus offer promise as a long-life ion detection solution[11], though these multiple conversion stages present a challenge for fast time response compared to more conventional methods.

An advance on reflectron-ToF mass spectrometry has been the development of multi-reflection analyzers that generate a much longer, folded ion path allowing for much higher achievable resolving power[12-15]. Particularly relevant to is the recently described Astral™ analyzer[16-17], which compresses a 30 m ion path onto a tabletop sized analyzer, and into which the detector developments described here were integrated. The order of magnitude longer ion path relaxes the overwhelming requirement for sub-nanosecond detector response and allows some sacrifice of single-ion pulse width in return for the implementation of other beneficial technologies such as an optically coupled PMT and signal pre-amplification.

The Astral analyzer also imposes a particular demand on the detector as ions are accumulated in an ion trap prior to pulse-extraction into the analyze[18]. Unlike traditional orthogonal extractors, such extraction traps have no issues with duty cycle or transmission, but operate with a slower repetition rate, for example with 200 Hz instead of ~10 kHz. This means that a single shot must have sufficient ions to generate a full mass spectrum, up to 50,000 ions per cycle and even thousands of ions in one species arriving at the same time at the detector. This imposes a challenging requirement for dynamic range, where detectors matched to an 8, or more recently 10-bit analogue to digital convertor (ADC) might manage barely 2 orders of magnitude dynamic range[19].

In this article we describe an ion detection device integrated into the Astral analyzer, termed HDR detector for its high dynamic range. This incorporates several unusual technologies, including an optically coupled detector with a 270º BxE focused path for secondary electrons and a PMT, an electrostatic tilt correction device, 10 keV post-acceleration, and splitting of output signal into separate channels with pre-amplification.

EXPERIMENTAL SYSTEM

For evaluation, the HDR detector was installed into the Astral analyzer module of a prototype Thermo Scientific™ Orbitrap Astral™ mass spectrometer, a hybrid instrument incorporating quadrupole, Orbitrap™ and Astral analyzers that has been previously described[16]. The Astral analyzer itself is shown in Figure 1a, and while a detailed description may be found in previous publication[17], it is a form of multi-reflection analyzer. Electrosprayed ions are quadrupole isolated, then accumulated and optionally fragmented in the ion processor[18], prior to potential lift to 4 kV and pulsed extraction. The extracted ions are focused and directed by the injection optics into the mirror system, where they oscillate between the opposing rectangular mirrors and drift down their length to form a zig-zag ion path. Asymmetry, or tilting of the mirrors relative to one-another, applies a counter force reducing the ions' drift velocity and ultimately halting and reversing it, so that ions are returned back to the post-accelerator, where they are accelerated to 14 keV and focused onto the detector surface. The ion foil compensation electrodes serve to both counter ToF aberrations induced by the converging ion mirrors and improve the spatial focus of the returned ions, maximizing transmission through the analyzer.

The full detector assembly model is shown in Figure 1b, including a post-accelerator and integrated tilt corrector, while the detector alone is shown in Figure 1c. The post-accelerator is a stack of 5 rectangular-apertured electrodes separated by a chain of 1 GΩ resistors (chosen to minimize current flow) that generates a potential gradient from ground to -10 kV in positive ion mode, so that ions travelling through the aperture series are accelerated from 4 to 14 keV.

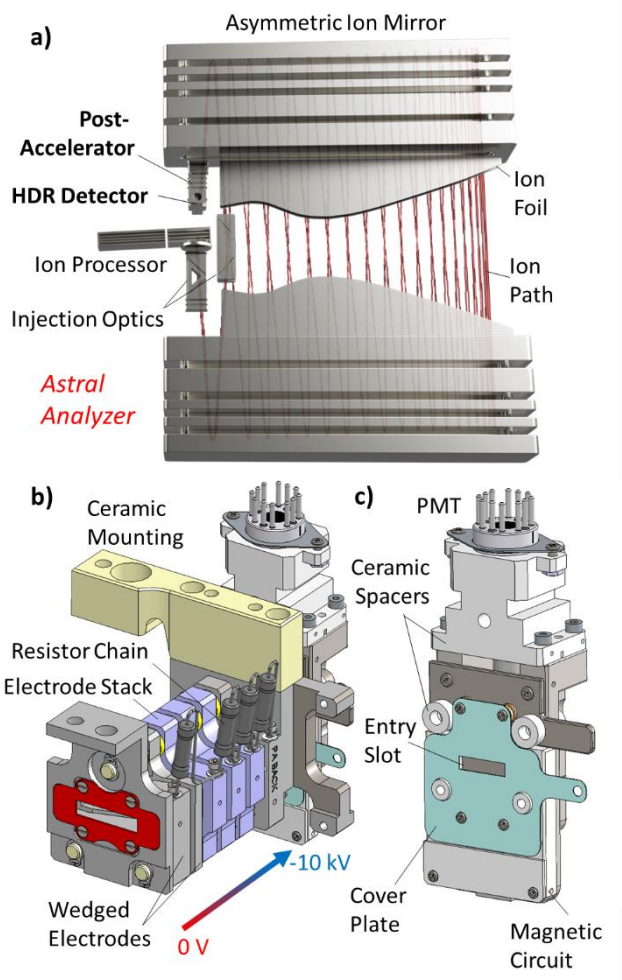

Figure 1. a) Ion optical arrangement of the Astral mass analyzer. b) The complete post-accelerator and detector assembly. c) Model of the detector alone.

Both the first grounded electrode, and an additional electrode with its own independent power supply, interleaved between the first and second in the voltage chain, are wedged to produce a field at about 30° to the ion trajectory. This angled field works to deflect the ion beam[20], a mechanism used advantageously in other deflectors in the Astral analyzer[21]. A second, usually unwanted, side effect of this process is that the orientation of the ion packet's focal plane becomes tilted in proportion to the

strength of the field. Normally this is a problem with the use of deflectors in the design of multi-reflection ToF analyzers, as the deflector can cause the ion focal plane to de-align from the detector surface, generating a large time-of-flight aberration with ion position and crippling resolving power.

In this case however this "deflector" is so close to the detector surface that the impact of the trajectory change is generally negligible, and instead the controllable tilting of the focal plane is used to align it to the detector surface[7]. This tilt corrector device in principle allows compensation of small mechanical errors in the analyzer, such as micron-level errors in mirror convergence. Other methods of focal plane tilt correction have also been proposed including use of wedge fields within the mirror system[22], the initial acceleration[4], and multipoles[6].

The detector itself is mounted to the final -10 kV plate of the post-accelerator, separated by insulating ceramic spacers. A cross section of the detector is shown in Figure 2a, along with applied voltages. The detector combines sequential conversion of ions to secondary electrons, to photons, then back to electrons for electron-multiplication in an optically coupled photomultiplier tube (PMT). From exiting the post-accelerator, ions pass through a 2 mm entrance slot in the detector's cover plate, held at -9.8 kV, before striking the conversion dynode below to generate secondary electrons. A slot was chosen over the more conventional grid thanks to the narrow incoming ion packet, which helped to minimize ion loss and formation of false-positive secondary ions. Having a small voltage step down from the post-accelerator to the entrance slot also served to prevent negative secondary ions escaping back into the post-accelerator, where they could be accelerated up to 10 keV and generate a harmful chain reaction of additional unwanted ions and electrons.

The conversion dynode is held at +500 V from the cover plate, defining part of the electric field through which secondary electrons navigate. A magnetic circuit composed of two neodymium magnets mounted at the end of the detector, and two mild steel arms running up the sides of the device, generate a 300 G strength magnetic field orthogonal to the electric field. Analyte ions enter the detector through the entry slot, hit the conversion dynode and produce secondary electrons. These electrons make a circular (270 degree) path in the ExB field and strike the inorganic scintillator, producing photons. The scintillator has a potential of +6 kV relative to the conversion dynode.

The photons (approximately 30 per impinging electron) travel down a short glass light guide to the PMT (R98880U, Hamamatsu Corporation), with the collection efficiency of about 60%. The PMT incorporates a photocathode with a quantum efficiency of 30% averaged over the incident photon wavelength emission spectrum (so 30 photons * 60% * 30% ~5 photoelectrons per incoming electron are provided). The detector exhibits a 1.25 ns full-width half-maximum output pulse for a single incident photon, and its dynode series generates a gain of ~10^4 at a typical operating voltage of -550 V[23]. Voltages are supplied to the legs of the PMT's dynodes via a custom-made resistive divider board directly mounted to them, which also receives the ground coupled output signal and forwards it to the pre-amplifier.

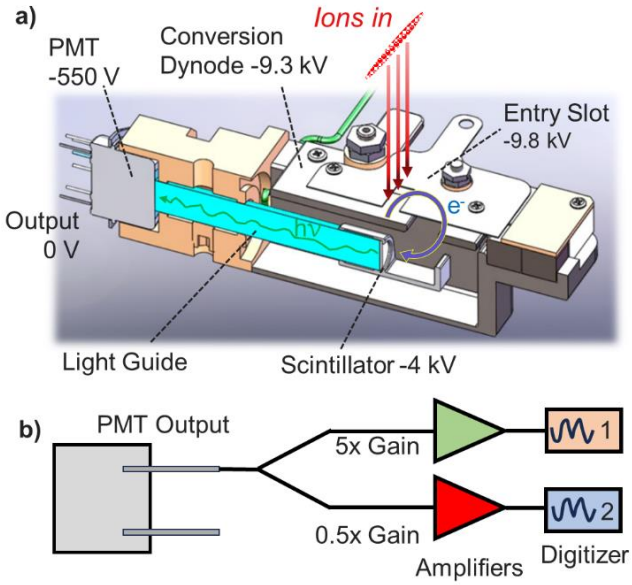

Figure 2. a) Cross-section of the detector. b) Schematic of signal path.

The signal handling after the PMT is illustrated in Figure 1b. The pre-amplifier splits the signal from the PMT output into two channels, each with their own amplifier. In typical ToF systems with 3 or 4 m flight paths, the need to maintain sub-ns peaks creates a high bandwidth requirement for any electronic amplifier, while the far longer flight times of the Astral analyzer are more tolerant. One channel may thus be amplified quite heavily, to 5x the original level with 500 MHz bandwidth, while the other channel is attenuated to 0.5x. Both low gain and high gain outputs are fed into separate 2 gigasample per second, 14-bit ADC channels incorporated into a dual-channel digitizer (Acqiris), which applies noise thresholding and transfers data from the two channels to the instrument's embedded PC.

The low and high gain channel data are received independently. The high gain channel produces sensitive features, with much greater signal to the digitizer's noise, but an order of magnitude lower saturation level. A combined spectra is constructed on the fly by replacing saturated data from the high gain channel with their equivalents from the low gain channel. Splitting signal between dual ADC channels with differing gain to enhance dynamic range has been previously described for short ToF analyzers[24]. Figure 3 shows how the combination of channels expands the dynamic range of an example spectrum generated from Pierce™ FlexMix™ calibration solution, with the saturated data from the high gain channel in blue overridden by the equivalent low gain data in green. The digitizer channels have a maximum voltage range (50 Ω termination) of a little under 500 mV, and with a 10x gain difference the low gain channel extends this limit almost to an effective 5 V, though this is actually equivalent to 1 V measured at the output of the PMT (1 V attenuated by 2x at the pre-amplifier to 0.5 V at the digitizer low gain channel input, and then scaled to 5 V due to the 10x gain difference to the high gain channel). That the PMT output is linear to >1.6 V shows that there is some space for further optimization, while the 10x gain difference between channels proved to be working.

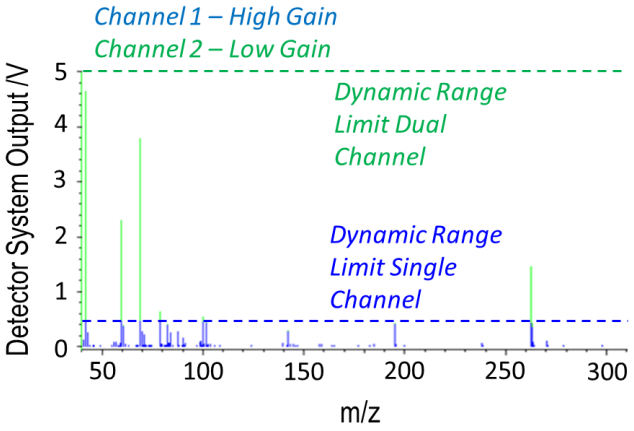

Figure 3. FlexMix calibration mixture mass spectrum showing splitting of signal between high and low gain channels.

A series of experiments were performed with admitted FlexMix ions, typically the MRFA peptide at *m/z* 524, to calibrate and evaluate the various technologies of the detection system. Some experiments requiring multiply charged or high *m/z* ions were otherwise performed with <1 μM solutions of ubiquitin, angiotensin or AHFP dissolved in 1:1 acetonitrile and water.

RESULTS AND DISCUSSION

Tilt Corrector: The impact of the tilt corrector was measured by scanning its applied potential and monitoring the resolution of a MRFA ion peak at *m/z* 524. The function of the tilt corrector is shown in Figure 4a, and the impact of changing the potential on the resolution of the MRFA peak in Figure 4b. The wedged electrode pair creates regions of lower and higher potential, corresponding to slower and faster ion velocity. The proportion of the time an ion spends in each region is dependent upon the position of the ion within the tilt corrector, so that the ions average velocity varies as a function of position, as does the time-of-flight of ions through the device. Consequently, the focal plane of the ions becomes tilted by passage across the tilt corrector.

In this test, the optimum tilt corrector potential was found to be -1000 V, improving resolving power from 60k at 0 V to >100k. In other instruments, the optimum varies widely depending on the level of mechanical error. One limitation of the existing design is that the allowable voltage range is only -2000 to +500 V without risking electrical breakdowns, and often a stronger positive potential would be desirable. Though rare, anomalous peak shapes have also sometimes been associated with extremes of the tilt corrector voltage, which may possibly be associated with 3D field perturbation as ions approach the side walls of the post-accelerator. Fortunately, the tilt corrector is not the only correction available for the most common error, micron-level misalignment of the ion mirrors, and adjustment of the ion foil electrodes to change the number of oscillations by ±1 has also proven to be a useful method when error exceeds the range of the tilt corrector.

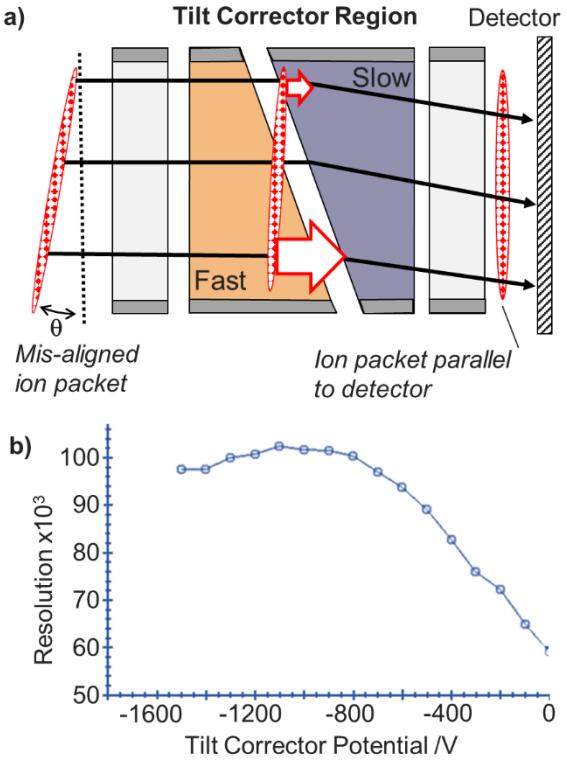

Figure 4. a) Operation and b) tuning of the tilt corrector.

Peak Quality and Noise: A significant issue of ion detectors operating at a high potential, that are capacitively coupled to a grounded output, is low percent-level ringing after any strong peak that carries on often for some microseconds. In a mass spectrum this creates the impression that any strong peak has a train of secondary peaks following it which makes low-lying higher *m/z* features more difficult to reliably detect and assign.

To test the quality of recorded peaks, the ion mirror voltages were set 200 V away from their optimum levels to compromise focusing, so that MRFA ions were slightly scattered and the MRFA peak appeared as distinct single ions at a shifted apparent *m/z* of 534. The detector voltage was also increased to make single ion signals suitably intense. This is a challenging test, as the very narrow single ion pulses expose short term ringing that would be obscured with multiple overlapping ions. Figure 5 shows profile spectra of several single ion peaks, and it may be seen that the peaks are of good quality, with sharp rise and fall. Nanosecond-level ringing quickly settles after the peaks, and in three of the peaks is barely noticeable, while for the largest peak a low percent level dip and rise is observable. Typically, the noise subtraction threshold was set to 3.5-4 mV for the high gain channel, calibrated to 6x the electronic noise standard deviation. There was no longer term, microsecond level perturbation observed for strong peaks of single or multiple ions.

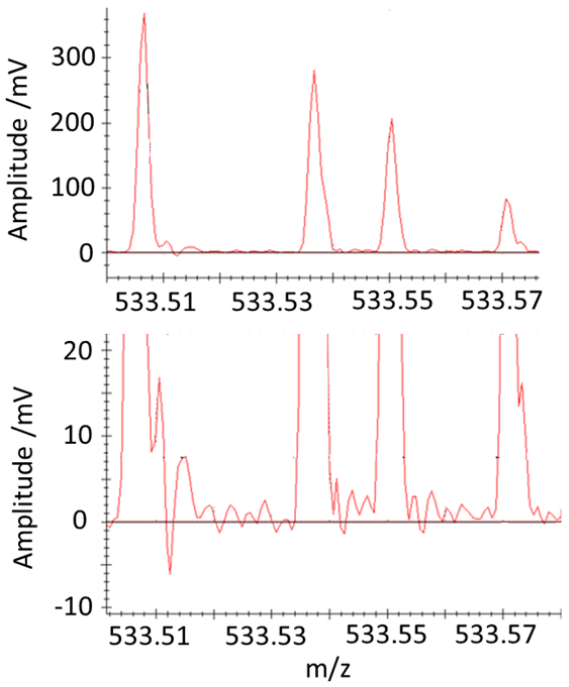

Figure 5. Defocused MRFA single ion peaks with a zoomed view of the baseline showing low after-peak ringing and noise.

Gain Calibration: Evaluation via single ions also allows the calibration of the applied PMT potential and thus detector gain. As a general rule, insufficient gain leaves the detector insensitive to most or all single ion signals. Excessive gain on the other hand compromises the detector's dynamic range, and also risks leaving the detector sensitive to single photon signals creating additional unwanted background peaks. As detector lifetime is also related to output current, this will also be reduced by high gain. As a compromise we choose a detector gain which is just sufficiently sensitive to detect most single ion signals, say a roughly ~80% detection probability based on signal/noise and the single ion intensity distribution. It is also important to have a good understanding of the ion current, so that ion accumulation time in the ion processor can be correctly set to properly populate the analyzer, a process known as automatic gain control[25].

A well-known detector calibration method is to count the change in the number of single ion signals with a scan of the applied detector potential and look for a plateau as detection probability becomes efficient,[26] as in Supplemental Figure 8. In this case, a good evaluation of the signal area and thus number of ions in each peak is also desirable. The detector was calibrated first by measuring MRFA single ions at a high gain and with the ion mirror voltages set to defocus the ion packet into a spread of single ions. The analyzer was then switched back to a focusing mode, and the PMT voltage scanned down while the intensity of the multiple ion peak was monitored. The advantage here is that the multiple ion peak is completely detected at and below the optimum gain value, whereas an increasing number of single-ion peaks falls below the detection threshold for lower gain values leading to a bias of the mean area of the detected peaks compared to the true value.

Figure 6a shows a histogram of single ion pulse widths recorded during the gain calibration experiment. In this case the median single ion pulse FWHM, and thus the time response of the detection system, was just under 1.9 ns. This is slow compared to regular <1 ns time-of-flight detectors, but tolerable with the long flight times of the Astral analyzer. Figure 6b shows a separate analysis made without the pre-amplifier and a different version of the PMT voltage divider, showing a time response better than 1.6 ns. While this difference has some advantage for resolving low *m/z* ions, where ion arrival FWHM dips below 2 ns, the benefit of these electronics outweighs the cost to peak width.

Figure 6c compares the measurement of single ion area with PMT potential from a direct measurement of defocused single ions, and the indirect measurement with a focused multiple ion peak. The two calibration curves diverge considerably from 500 V down, as a growing proportion of low-level single ions generate pulse intensities below the detection threshold and cease to be detected, leading to the aforementioned bias. A typical suitable value for the single ion area is ~1.5×10^{-11} Vs, relating to ~7.5 mV peak height and approximately 80% single ion detection efficiency on the high gain channel (see Supporting Information for more detail). An automated procedure based on this method has been described[27].

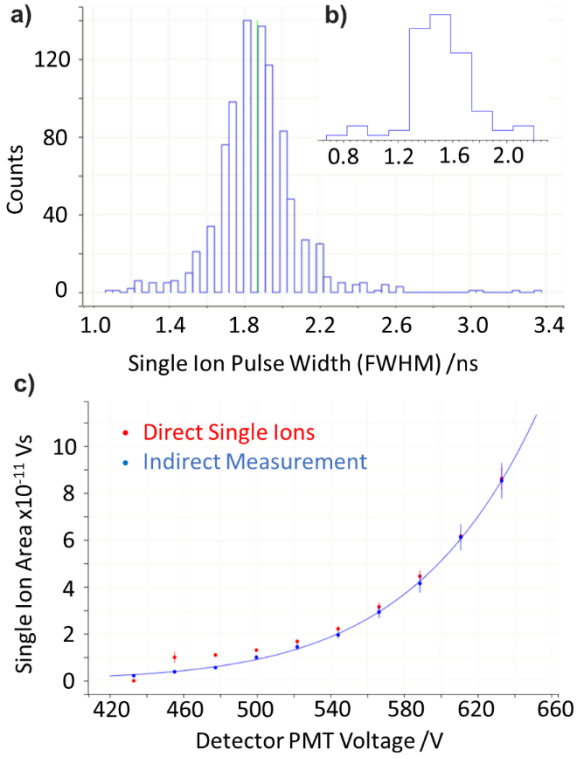

Figure 6. Single ion peak width distribution (full width half maximum) measured in a) the complete system and b) without pre-amplifier electronics. c) Gain calibration measurement of defocused single ion peak area measured both directly and inferred from a refocused peak.

Relationship between Intensity, Charge State and *m/z*: A good understanding of the number of ions in the detector peak required further knowledge of how peak intensity varies with *m/z*, and with differences in charge state. To the authors' recollection, such corrections are not normally made in mass spectrometers, despite the potential to perturb measurement of the amount of sample present. It is well known that the efficiency of conversion of ions to secondary electrons varies strongly

with charge state and ion velocity[28-32] which for the 14 keV kinetic energy (of singly charged ions) depends strongly on mass.

Single ion areas were recorded of various charge states of ions found in FlexMix, angiotensin and ubiquitin solution, while the trend with m/z was measured with FlexMix and the wide mass spread of AHFP cluster ions. Figure 7a shows the trend of single ion area (SIA) with m/z, while Figure 7b shows the trend with charge state (the m/z dependency from Fig. 7a already factored in). In both depictions, a correction is applied for estimation of undetected ions which produce no secondary electrons (compare black and red markers in Fig. 7a, see Supporting Information for more detail).

A linear trend between signal intensity and charge state is observable (dashed line in Fig. 7b). Therefore, a basic model for the SIA at charge state z is to multiply the calibrated SIA for singly charged ions by z (see dotted line in Fig. 7b). For larger charge states, ringing effects and unwanted fragmentation, at the time of the experiment, made the gain measurements more involved and subject to an increasing upward bias of the SIA. This might help explain the discrepancy of the basic model and the best fit line to the data points (increasing with charge). For the very same reason, the last two data points were omitted from the best fit. At least to this modest range of charge states, this means no special correction need be applied as the signal is proportional to the number of charges.

The relationship between intensity and m/z shown in Figure 7a is much more complex; initially rising to a maximum at m/z 140 and then decaying exponentially. These datapoints include a modelled correction for the impact of the proportion of undetected ions, which produce 0 secondary electrons33. This becomes increasingly important above m/z 2000, and at m/z 6000 detection efficiency is estimated to fall by 50% due to these zero electron events. Furthermore, singly charged single ions at this *m/z* are also much less likely to be detected due to the peak intensity failing to exceed the noise threshold for a detector gain optimized for *m/z* 524. Fortunately, in most biological applications such high *m/z* ions are typically also multiply charged, though there may be some applications where running at higher detector gain is suitable. Physically, the impact velocity v of the incident ions is the most important degree of freedom alongside the charge state. The trend of measured SIAs was therefore fitted to an empirical function F_v,

$$F_v = a v^b \exp\left(-\frac{v}{v_0}\right)$$

where a, b and v_0 are best fit parameters of values a=1.37x10^{-5} mVns (m/s)$^{-b}$, b=0.74 and v_0 =93754 m/s, respectively. This velocity is coupled to the mass m of incident ions by the kinetic energy equation $T = \frac{1}{2} m\, v^2$, where the ion picks up its kinetic energy by traversing the corresponding acceleration voltage. Therefore, the mass dependent representation of the fit function is

$$F_m = (\sqrt{2T})^b a m^{-b/2} \exp\left[-\frac{(2T)^{\frac{1}{2}} m^{-\frac{1}{2}}}{v_0}\right]$$

There is substantial deviation of points from the trendline, due to the experiment's practical difficulty. However, it is thought that the resultant corrected measurements are greatly improved versus uncorrected data, also indicated by a greater similarity between Astral and Orbitrap spectra after correction. Colloquially it is understood that ion trap mass spectrometers, and presumably triple quadrupoles, do not suffer such strong mass dependencies, which may be down to their generation and measurement of secondary ions in addition to secondary electrons. Use of secondary ions is undesirable in the Astral analyzer because of the requirement for nanosecond time response, like any high-resolution time-of-flight analyzer.

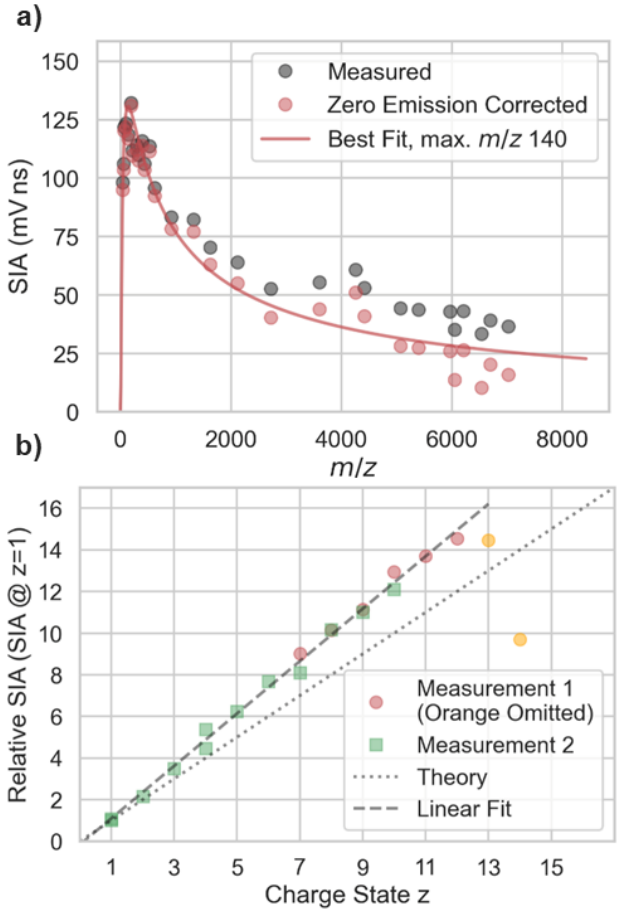

Figure 7. Measurement of relationship between single ion peak area with a) m/z ratio recorded with FlexMix and AHFP ions and b) charge state over two measurements of angiotensin and ubiquitin ions. In the simplest theory, doubling the charge should double the SIA, so the relative SIAs should match the angle bisector line x=y as a function of the charge state ("Theory"), together with a least square fit line ("Linear Fit"). See text and Supporting Information for more detail.

Dynamic Range: Figure 8 shows profile spectra of isolated multiple ion MRFA peaks under increasing numbers of ions in the peak, generated by adjusting the ion accumulation time in the ion processor as an evaluation of dynamic range. Both ADC channels are shown. For a 250-ion peak, the channels are almost equivalent, though at this 450 mV level, the high gain channel is already saturated and demonstrating some non-linearity. Slight non-linearity in the pre-amplifier means that the switching point is better set at ~400 mV, a little below the actual limit of the ADC. There are no abnormalities in the peak shape beyond some typical minor non-gaussian tailing.

For the 1000 ion peak the high gain channel is extremely saturated, and the low gain channel is always used. The peak shape here is still good, though resolving power falls somewhat due to Coulomb repulsion. At 5000 ions, although the peak is

clearly more intense, the low gain channel has not become saturated to the ~4.5 V equivalent level. Here space charge effects have continued to broaden the peak, which is obviously deleterious for resolution, but also very helpful for dynamic range. This serendipitous effect extends the in-spectrum dynamic range well beyond what might be anticipated just by looking at the bit-depth of the digitizer system.

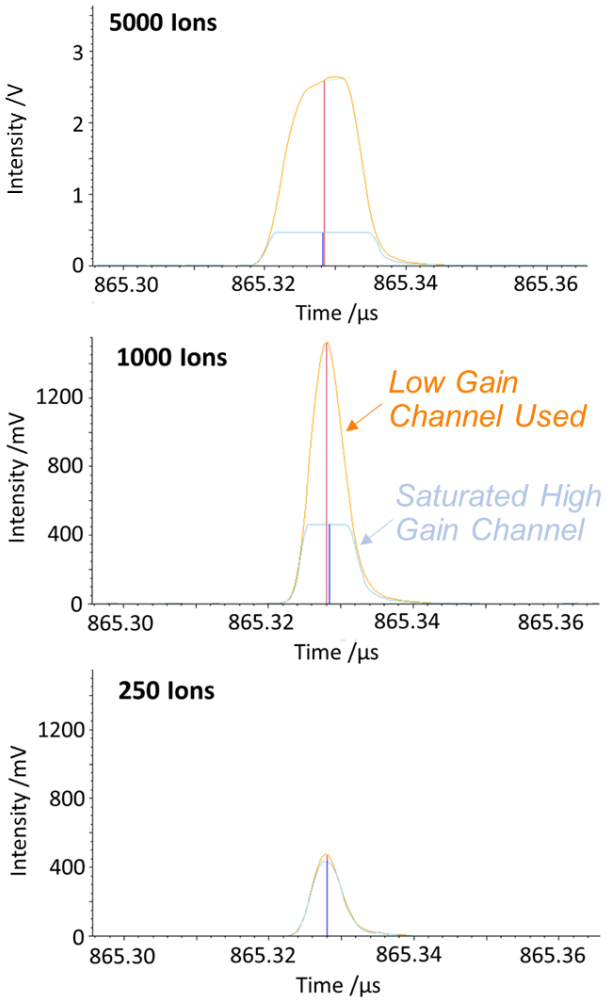

Figure 8. *m/z* 524 peaks for the two ADC channels at various numbers of detected ions, showing saturation of high gain channel from 250 to 1000 ions in peak, and peak broadening at high intensity under increasing space charge.

The dynamic range however remains strongly mass dependent. Figure 9a shows linearity plots generated by scanning the ion accumulation time, or ion number, for a range of different *m/z* peaks. Taking the minimum number of detectable ions as 1 (single ion detection), the dynamic range is then representable by the maximum number of ions detected before intolerable non-linearity sets in. The high *m/z* 2122 Ultramark sees a substantially greater linear dynamic range than the *m/z* 524 MRFA, more than 4-orders of magnitude in a single shot. Low *m/z* 142 however has a much narrower time spread, closer to the single ion time response, and thus the same signal area results in a higher voltage peak that more rapidly saturates the digitizer. Thus, at low *m/z*, linear dynamic range is reduced to 5000. This is one area where a narrower detector response might be helpful, as it allows single ion detection at lower PMT gain thus later saturating the digitizer.

Figure 9b shows another challenging test, in which the *m/z* 524 MRFA isotopic cluster is injected with 10,000 ions in the parent ion, a saturated peak, and the presence of the lesser isotopes and background ion signal recorded in a single shot. Low lying species at the 0.01% level are visible, a testament to the detector's dynamic range, though it is difficult to assign isotopic peaks from background at such low level. One minor observation is that there are small dead spots to the right of every intense peak, a combination of high *m/z* tailing of peaks, exacerbated by recovery time of the high gain channel pre-amplifier.

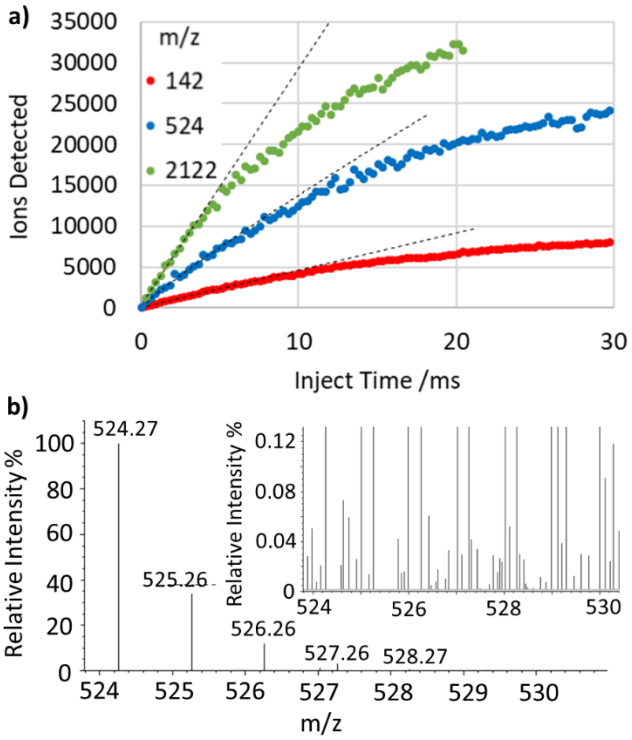

Figure 9. a) Linearity of signal response to increasing number of isolated ions of differing *m/z*. b) Single shot 10,000 ion injection of MRFA parent ion, showing surrounding isotopic envelope and low-level background peaks.

Detector Lifetime: The final critical evaluation was of the lifetime of the detector since the great benefit of hermetically sealed PMTs is their resistance to ageing effects. The detector was installed into a test assembly, a small time-of-flight mass spectrometer fed by an electron impact source generating *m/z* 614 ions from PFTBA vapor. The charge delivered and the single ion pulse height distribution were regularly monitored. After 4.8 µC was delivered, equivalent to approximately a year's use in standard omics applications, the average single ion area had reduced from 687 to 666 arbitrary units, a loss of around 3%. An additional measurement at 5.6 µC caused a drop to 639 a.u, a trifling 7% reduction in gain. This allows one to project a detector lifetime of several years, certainly far more than the interval between regular service. The stability of the gain over time is also important from the perspective of needing only occasional calibration, and the sealed PMT is immune to disturbances after venting and pumping the analyzer, speculated to be caused by adhesion of water to dynode chain surfaces.

The high lifetime demonstrated implies that the 5x amplification of the high gain channel may not really be necessary, and there may be room to reduce or remove this amplification, allowing instead improvements in bandwidth, linearity or recovery time. Though to do so might reduce the pre-amplifier to serve as a sacrificial component that merely protects the vastly more expensive digitizer from damage caused by potential electronic breakdowns.

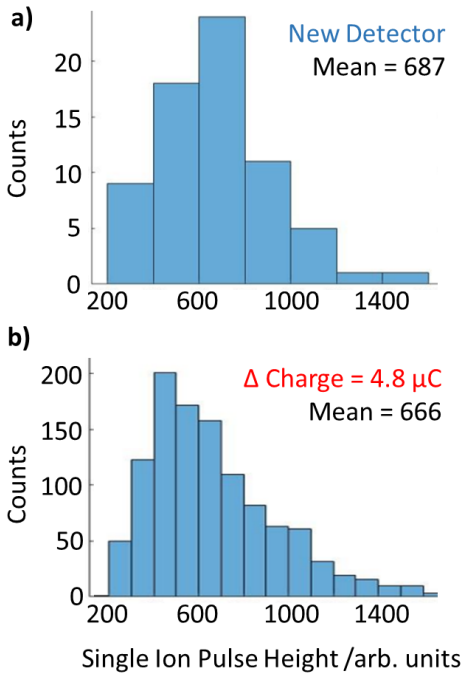

Figure 10. Single ion pulse intensity histogram measurements recorded on a) a new detector and b) after 4.8 µC of charge detected.

CONCLUSION

A high dynamic range detection system has been implemented into the Astral analyzer, incorporating 10 kV post-acceleration with integrated ion packet tilt corrector, BxE conversion dynode with paired scintillator and photomultiplier tube, and dual channel acquisition. The detector has been shown to produce 4-orders of magnitude single shot dynamic range, except for low *m/z* ions, along with efficient single-ion detection, low noise and spectral artifacts, and with a lifetime projected to approach that of the instrument.

ASSOCIATED CONTENT

Supporting Information

Supporting Information is available covering additional details of the hardware, simulation and experiments.

AUTHOR INFORMATION

Corresponding Author

Hamish Stewart – Thermo Fisher Scientific, 11 Hannah Kunath Straße, 28199 Bremen, Germany
Phone: +49 (0)1737284255
Email: hamish.stewart@thermofisher.com

Author Contributions

The manuscript was written through contributions of all authors. All authors have given approval to the final version of the manuscript.

Notes

The authors declare the following competing financial interest(s): SS, BM, AW and SK are employees of El-Mul Technologies Ltd., the manufacturer of the ion detector. All remaining authors are employees of Thermo Fisher Scientific, the manufacturer of instrumentation used in this research.

ACKNOWLEDGMENT

The authors would like to acknowledge the advice and support of colleagues throughout Thermo Fisher Scientific and El-Mul Technologies Ltd.

REFERENCES

[1] Mamyrin, B. A. Time-of-flight mass spectrometry (concepts, achievements, and prospects). *Int. J. Mass Spectrom*. **2019**, *206* (3), 251-266.

[2] Guilhaus, M., Selby, D., & Mlynski, V. Orthogonal acceleration time-of-flight mass spectrometry. *Mass Spectrom. Rev.* **2000**, *19* (2), 65-107.

[3] Chernushevich, I. V., Loboda, A. V. and Thomson, B. A. An introduction to quadrupole–time-of-flight mass spectrometry. *J. Mass Spectrom*. **2001**, *36* (8), 849-865.

[4] Hoyes, B. H., Langridge, D. J. and Wildgoose, J. Electrostatic gimbal for correction of errors in time-of-flight mass spectrometers. *United States Patent US8921775B2*. **2014**.

[5] Dresch, T. Mass resolution by angular alignment of the ion detector conversion surface in time-of-flight mass spectrometers with electrostatic steering deflectors. *United States Patent US5654544A*. **1997.**

[6] Stewart, H., Gill, M. and Giles, R. Time of flight mass spectrometer. United States Patent US10269549B2. **2019**.

[7] Grinfeld, D., Hock. C. and Stewart, H. Ion front tilt correction for time of flight (TOF) mass spectrometer. *United States Patent US11158494B2*. **2021**.

[8] Wiza, J. L. Microchannel plate detectors. *Nucl. Instrum. Methods*. **1979,** *162*, 597-601

[9] Stresau, R., Hunter, K., Shields, W., Raffin, P. and Benari, Y. A new class of robust sub-nanosecond TOF detectors with high dynamic range. *Proceedings of the 54th ASMS Conference on Mass Spectrometry and Allied Topics*, **2006**, Seattle, Washington.

[10] Cutter, D. A., Hunter, K., Paterson, P. J. K. and Stresau, R. W. The "AGING" Mechanism in Electron Multipliers and Operating Life. *Proceedings of the 42nd ASMS Conference on Mass Spectrometry and Allied Topics*, **1994**, Chicago, Illinois.

[11] Verenchikov, A. N. and Vorobyev, A. Right angle time-of-flight detector with an extended lifetime. *United States Patent US10770280B2*. **2015.**

[12] Wollnik, H. and Przewloka, M. Time-of-flight mass spectrometers with multiply reflected ion trajectories. *Int. J. Mass. Spectrom. Ion Processes*. **1990**, *96* (3), 267-274.

[13] Sudakov, M., & Kumashiro, S. TOF systems with two-directional isochronous motion. *Nucl. Instrum. Meth. A*. **2011**, *645* (1), 210-215.

[14] Verentchikov, A. N., Yavor, M. I., Hasin, Y. I., & Gavrik, M. A. Multireflection planar time-of-flight mass analyzer. I: An analyzer for a parallel tandem spectrometer. *Tech. Phys.* **2005**, *50* (1), 73-81.

[15] Nazarenko, L.M., Sekunova L.M., Yakushev E.M. Time-of-flight mass spectrometer with multiple reflections, *Soviet Patent No. SU1725289*. **1989**.

[16] Stewart, H., Grinfeld, D., Giannakopulos, A., Petzoldt, J., Shanley, T., Garland, M., ... & Hock, C. Parallelized Acquisition of Orbitrap and Astral Analyzers Enables High-Throughput Quantitative Analysis. *Anal. Chem*. **2023,** *95* (42), 15656-15664.

[17] Grinfeld, D., Stewart, H., Balschun, W., Skoblin, M., Hock, C., & Makarov, A. Multi-reflection Astral mass spectrometer with isochronous drift in elongated ion mirrors. *Nucl. Instrum. Meth. A*. **2024**, 1060, 169017.

[18] Stewart, H., Grinfeld, D., Wagner, A., Kholomeev, A., Biel, M., Giannakopulos, A., ... & Hock, C. A Conjoined Rectilinear Collision Cell and Pulsed Extraction Ion Trap with Auxiliary DC Electrodes. *J. Am. Soc. Mass Spectrom*. **2023,** *35* (1), 74-81.

[19] Fjeldsted, J. Time of Flight Mass Spectrometry Technical Overview. *Agilent Technologies 5989-0373EN*, **2003**, https://www.agilent.com/cs/library/technicaloverviews/Public/5989-0373EN%2011-Dec-2003.pdf.

[20] Glikman L. G. & Goloskokov Y. V. A new class of electrostatic systems which keep plane homogeneous charged-particle beams exactly parallel. *Tech. Phys. Lett*. **1998**, 24, 772.

[21] Stewart, H., Grinfeld, D., Hagedorn, B., Ostermann, R., Makarov, A., & Hock, C. Proof of principle for enhanced resolution multi-pass methods for the Astral analyzer *Int. J. Mass Spectrom*. **2024**, *498*, 117203.

[22] Verenchikov, A. N., Yavor, M. I., & Pomozov, T. V. Control of time front tilts in planar multi-reflection time-of-flight mass analyzers by local wedge fields. *Int. J. Mass Spectrom*. **2021**, *469*, 116680.

[23] Metal package photomultiplier tube R9880U series. *Hamamatsu Photonics*. **2022**.

[24] Beavis, R. C. Increasing the Dynamic Range of a Transient Recorder by Using Two Analog-to-Digital Converters, *Anal. Chem*. **1996**, *7*, 107-113.

[25] Schwartz, J. C., Zhou, X. & Bier, M. E. Method and apparatus of increasing dynamic range and sensitivity of a mass spectrometer. *United States Patent US5572022A*. **1996**.

[26] Prohaska, T., Irrgeher, J., Zitek, A., & Jakubowski, N. (Eds.). Sector Field Mass Spectrometry for Elemental and Isotopic Analysis. *Royal Society of Chemistry*. **2014**.

[27] Stewart, H., Petzoldt, J., Hagedorn, B. & Grinfeld, D. Method of gain calibration. *United States Patent Application US20220367165A1*. **2022**.

[28] Beuhler, R. J., & Friedman, L. A model of secondary electron yields from atomic and polyatomic ion impacts on copper and tungsten surfaces based upon stopping-power calculations. *J. Appl. Phys*. **1977**, *48* (9), 3928-3936.

[29] Liu, R., Li, Q., & Smith, L. M. Detection of large ions in time-of-flight mass spectrometry: effects of ion mass and acceleration voltage on microchannel plate detector response. *J. Am. Soc. Mass Spectrom*. **2014**, *25* (8), 1374-1383.

[30] Sternglass, E. J. Theory of secondary electron emission by high-speed ions. *Phys. Rev*. **1957**, *108* (1), 1.

[31] Westmacott, G., Ens, W., & Standing, K. G. Secondary ion and electron yield measurements for surfaces bombarded with large molecular ions. *Nucl. Instrum. Meth. B*. **1996**, *108* (3), 282-289.

[32] Schwartz, J. C., Quarmby, S. T. & Schoen, A. E. Why multiply charged ions do not cause space charge problems in a quadrupole ion trap. *Proceedings of the 46th ASMS Conference on Mass Spectrometry and Allied Topics*, **1998**, Orlando, Florida.

[33] Hagedorn, B., Mourad, D., Shanley, T., Stewart, H. & Dwivedi, A. Processing ion peak areas in mass spectrometry. *United States Patent Application US20240014021A1*. **2023**.